Field Oriented Control for an Induction Machine Based Electrical Variable Transmission

Joachim Druant, *Member, IEEE*, Frederik De Belie, *Member, IEEE*, Peter Sergeant *Member, IEEE*, and Jan Melkebeek *Member, IEEE*

***Abstract*—An electrical variable transmission (EVT) is an electromagnetic device with dual mechanical and electrical ports. In hybrid electric vehicles (HEV's) it is used to split the power to the wheels in a part coming from the combustion engine and a part exchanged with the battery. The most important feature is that the power splitting is done in an electromagnetic way. This has the advantage over mechanical power splitting devices of reduced maintenance, high efficiency and inherent overload protection. This paper gives a conceptual framework on how the torque on both rotors of the EVT can be controlled simultaneously by using a field oriented control scheme. It describes an induction machine based EVT model in which no permanent magnets are required, based on the classical machine theory. By the use of a predictive current controller to track the calculated current reference values, a fast and accurate torque control can be achieved. By selecting an appropriate value for the flux coupled with the squirrel-cage inter-rotor, the torque can be controlled in various operating points of powersplit, generation and pure electric mode. The conclusions are supported by simulations and transient finite element calculations.**

***Index Terms*—Electrical variable transmission, modeling, field oriented control**

I. Introduction

An electrical variable transmission (EVT) is an electromagnetic device with two mechanical (MP's) and two electrical (EP's) ports as can be seen in Fig. 1. The mechanical ports consist of a primary (driven) shaft, and a secondary (driving) shaft. The electrical ports are provided by two power electronic converters (PEC's) with a common DC-bus. The EVT serves as a power split device between the electrical and mechanical power sources.

In literature, the EVT is often found to be used in hybrid electric vehicles (HEV's). While full electric cars are limited by the unsatisfactory performance of battery technologies and the high cost of fuel cells [1], [2], the HEV needs only limited battery storage. These cars are powered both by an internal combustion engine and an electric motor. A power split device is required to split the power to the wheels in a part directly coming from the combustion engine and a part exchanged with the battery. This task is nowadays performed through a mechanical planetary gear [3], [4], for which two electric motor/generators are needed, each connected to a different shaft of the gear. The remaining shaft is connected to the combustion engine.

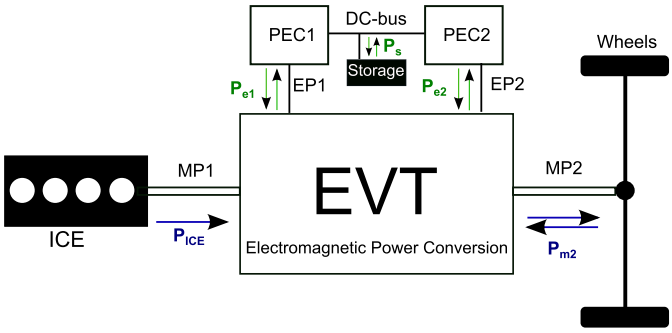

Fig. 1: Principle of a hybrid electric vehicle with electrical variable transmission (EVT). Also the possible power flows are indicated by arrows.

Also other topologies can be found in literature. In [5] a push-belt CVT is used as power split, while a flywheel is used to store some of the energy. In [6] a conventional automatic transmission replaces the planetary gear. Finally [7] compares the automated transmission with the continuously variable transmission. The power split in all topologies makes it possible to drive the engine in an energy-efficient region of the torque-speed map over a wide range of torques and speeds delivered to the wheels. The fuel consumption, the noise level and the emission of harmful gases from the vehicle can thus be reduced. Also, while braking, some of the braking energy can be recuperated and stored in the battery [8]. Although having a lot of advantages, this hybrid concept with a mechanical power split has some drawbacks inherent to mechanical gears. The most important are mechanical friction, the need for lubrication and sealing and the absence of overload protection. In addition, two electrical motor/generators are needed in the concept. The electromagnetic equivalent of this system combines the power split and the two electrical motors into one electromagnetic device called an electrical variable transmission (EVT) as can be seen in Fig. 1. There exist basically two types of EVT's, depending on whether or not permanent magnets are used.

Within the permanent magnet versions, different topologies can be found in literature. In [9] and [10] the magnetic

J. Druant was awarded a Ph.D. Fellowship from the Research Foundation-Flanders (FWO) in 2014 (email: Joachim.Druant@ugent.be). J. Druant, F. De Belie, P. Sergeant and J. Melkebeek are with the Electrical Energy Laboratory of the department of Electrical Energy, Systems and Automation (EESA) of Ghent University, B-9000 Ghent, Belgium. This research has also been carried out in the frame of project G.0083.13 of the Research Foundation-Flanders (FWO), and in the frame of Flanders Make.

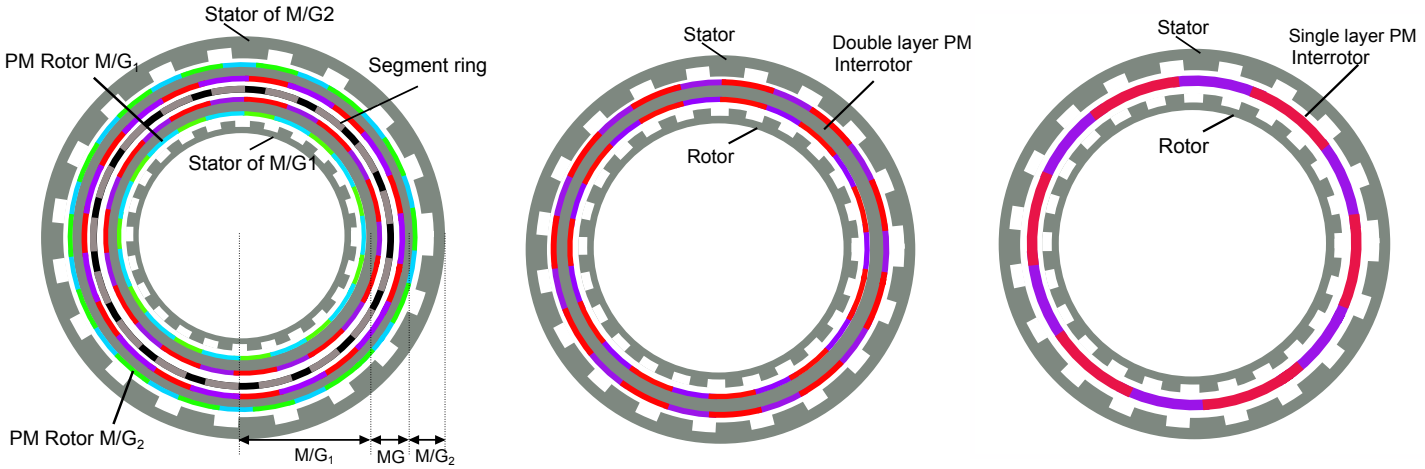

(a) EVT with magnetic gear (MG) inside [9], [10]. (b) EVT with double layer of PM's [11] (c) EVT with single layer of PM's [12]

Fig. 2: Schematics of the permanent magnet EVT.

equivalent of a planetary gear is used within the EVT as can be seen in Fig. 2a. Such a magnetic gear was proposed in [13], and can have a comparable power density as its mechanical counterpart according to [14]. Moreover, it has the advantage of high efficiency, absence of mechanical friction and wear, lower maintenance and inherent overload protection [15]. The two motor/generators are added concentrically to the magnetic gear as can be seen in the figure to form an EVT. The losses in a motor-integrated permanent-magnet gear are considered in [9] and [16]. They mainly consist of iron losses. Among the advantages of this kind of EVT are the high efficiency, high power density and the absence of slip rings. The mechanical construction is however complicated because of the three concentrically rotating elements. Also four layers of expensive permanent magnets are needed.

In [11], [17] another type of PM-EVT is considered avoiding the aforementioned drawbacks. However slip rings are needed to feed the wound inner rotor. The machine further consists of a wound stator, and an outer rotor (called inter-rotor in this paper) with a double array of permanent magnets. The topology can be seen in Fig. 2b. The yoke inbetween both layers of magnets is made thick so that the stator and rotor are magnetically decoupled. By controlling both the rotor and stator currents the torque on both the rotor and the inter-rotor can be controlled. Because of the decoupling, the control is identical as for conventional PMSM machines.

In [12] finally the inter-rotor is provided with a single array of PM's as can be seen in Fig. 2c. Now the stator and rotor are magnetically coupled, making the control more challenging. Depending on the speed of the rotor and inter-rotor, the electrical frequencies of stator and rotor need to be controlled in order to synchronize the different magnetic fields to one unique rotating field. Different operating points are considered in [18].

On the other hand, in the induction machine based EVT no permanent magnets are used. This machine was introduced in [19], [20]. In contrast to [21] here both rotors are electromagnetically coupled, since the inter-rotor yoke is made thin to save volume and weight. The machine can thus not be seen as two concentric conventional induction motors, but as one electromagnetically coupled device. With respect to the permanent magnet versions it has the advantage of lower cost since no expensive (rare earth) magnets need to be provided. Also the irreversible demagnetization risk of magnets is avoided [22]. Furthermore, the magnetic field can easily be weakened at high speeds in contrast to EVT's with permanent magnets. The disadvantage of this type of EVT is the higher joule loss due to on the one hand the inherent slip between the short-circuited rotor and the field and on the other hand due to the magnetization current.

In this paper the concept of this latter type of EVT is considered. The topology of the machine can be seen in Fig. 3, which consists of a stator, a short circuited squirrel-cage inter-rotor and a wound rotor with slip rings as also described in conference paper [23] where an equivalent scheme for this machine type is derived for modeling of steady-state operation. More specifically it is investigated in this paper how field oriented control can be applied to control the torque on both rotors along with the flux. The goal is to have the control working in the most energy-efficient way by selecting appropriate current vectors for stator and rotor. The currents are applied using voltage source inverters (VSI's) and an appropriate current controller. Drive lines of EVT's are often equipped with an overall energy management system choosing the optimal torque and speed on each shaft in order to fulfill the wishes of the driver while minimizing the energy consumption as presented in many recent articles [24]–[27]. To do this the machine needs to be controlled both in steady-state as well as in transient operation, according to the demands of the energy management, which is the subject of this paper. First a machine model for an induction machine based EVT is discussed, from which the torque

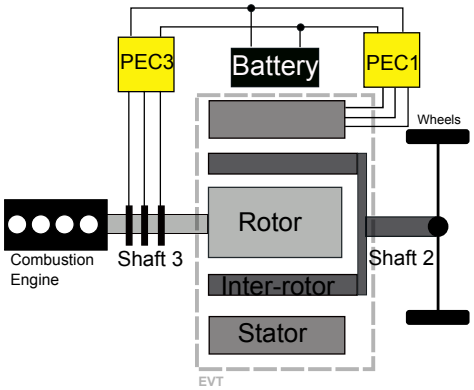

(a) Schematic of an EVT used in a hybrid vehicle.

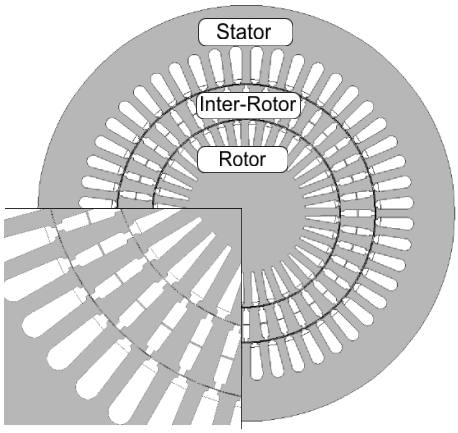

(b) Cross sectional view.

Fig. 3: Induction machine based electrical variable transmission.

on both rotors can be calculated. Further the proposed field oriented control scheme is explained, and the importance of choosing an appropriate inter-rotor flux is discussed. Finally, simulations results support the theoretical derivations. The aim is to give the results of a general concept study showing some possibilities of this kind of machine, and to encourage further investigation into this new technology.

II. The Induction Machine based Electrical Variable Transmission

A. General Description

The electrical variable transmission (EVT) considered in this paper is an electromagnetic device with two mechanical ports and two electrical ports. It can be seen as an induction machine with two concentric rotors. The stator is coupled through a power electronic converter (PEC) to the battery. The middle rotor is called the inter-rotor and is a squirrel-cage rotor. The most inner rotor finally is connected through slip rings and a power electronic converter to the battery. The stator and the two rotors are electromagnetically coupled. A schematic overview can be seen in Fig. 3a.

B. Electromagnetic Modeling

An analytical model for the EVT can be derived taking into account the following assumptions:

- A three phase symmetrical machine
- Sinusoidally distributed windings
- No skin- or proximity effect
- No saturation
- No influence of the slots on the field

When Faraday's and Ohm's law are considered in a reference frame rotating along with the magnetic field (synchronous qd-reference frame) equations (1) to (3) model the relation between the voltages applied to the terminals of the machine and the resulting currents. Note that there is only one rotating magnetic field. In each equations the flux is multiplied with the speed with respect to the field i.e. ω, $s_2\omega$ and $s_3\omega$ for the stator, inter-rotor and rotor respectively. The derivation is made using standard modeling techniques as for conventional induction motors [28]. The subscript 1 is used for the stator quantities, 2 for the inter-rotor and 3 for the rotor. The symbol R is used for the resistance, Ψ for flux linkage, and p is the Laplace operator. Note that although the inter-rotor is a short-circuited squirrel-cage rotor, an equivalent wound rotor is considered.

$$\begin{cases} V_{1q} = R_1 I_{1q} + p\Psi_{1q} - \omega\Psi_{1d} \\ V_{1d} = R_1 I_{1d} + p\Psi_{1d} + \omega\Psi_{1q} \end{cases} \tag{1}$$

$$\begin{cases} V_{2q} = 0 = R_2 I_{2q} + p\Psi_{2q} - s_2\omega\Psi_{2d} \\ V_{2d} = 0 = R_2 I_{2d} + p\Psi_{2d} + s_2\omega\Psi_{2q} \end{cases} \tag{2}$$

$$\begin{cases} V_{3q} = R_3 I_{3q} + p\Psi_{3q} - s_3\omega\Psi_{3d} \\ V_{3d} = R_3 I_{3d} + p\Psi_{3d} + s_3\omega\Psi_{3q} \end{cases} \tag{3}$$

ω is the pulsation of the magnetic field in a two-pole representation, whereas s is the slip of the considered rotor with respect to the field:

$$s_2 = \frac{\omega - \omega_2}{\omega} \tag{4}$$

$$s_3 = \frac{\omega - \omega_3}{\omega} \tag{5}$$

with ω_2 and ω_3 the inter-rotor and rotor pulsation respectively. N_p finally represents the number of pole pairs in the machine. The fluxes are defined as:

$$\begin{bmatrix} \underline{\Psi}_1 \\ \underline{\Psi}_2 \\ \underline{\Psi}_3 \end{bmatrix} = \begin{bmatrix} L_{11} & L_{12} & L_{13} \\ L_{12} & L_{22} & L_{23} \\ L_{13} & L_{23} & L_{33} \end{bmatrix} \begin{bmatrix} \underline{I}_1 \\ \underline{I}_2 \\ \underline{I}_3 \end{bmatrix} \tag{6}$$

which are the flux vectors linked to the stator, inter-rotor and rotor respectively considered in a reference frame rotating with pulsation ω:

$$\begin{cases} \underline{\Psi}_i = \Psi_{iq} + j\Psi_{id} \\ \underline{I}_i = I_{iq} + jI_{id} \end{cases} \tag{7}$$

with $i \in \{1, 2, 3\}$. The real axis is thus along the q-axis, while the imaginary axis is the d-axis. The parameters L_{ij} are determined using finite element calculations. A current vector $\underline{I}_i$, $i \in \{1, 2, 3\}$ of unity length is applied to the machine. The corresponding fluxes are the i^{th} column of the inductance matrix.

Finally using Lorentz' law, the torque on both rotors can be expressed as

$$\begin{cases} T_2 = \frac{3}{2} N_p (I_{2q}\Psi_{2d} - I_{2d}\Psi_{2q}) \\ T_3 = \frac{3}{2} N_p (I_{3q}\Psi_{3d} - I_{3d}\Psi_{3q}) \end{cases} \tag{8}$$

In (8) it is given that the torque magnitude and direction not only depend on the magnitude of the magnetic flux and the currents, but also on their relative angle. Thus, the concept of vector control applies for this kind of machine.

III. Torque control on a double rotor induction machine

As with field oriented control (FOC) on a conventional induction machine, the EVT is considered in a qd-reference frame rotating with the magnetic field. In this instantaneously synchronous reference frame all currents are DC-currents. The relative phase of the frame can be chosen freely. For simplicity of the equations, the inter-rotor flux Ψ_2 is chosen to be oriented along the negative d-axis. The mathematical expression for field orientation is thus:

$$\Psi_{2q} \equiv 0 \tag{9}$$

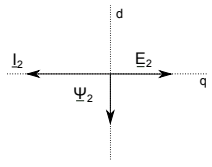

Fig. 4: dq-reference frame oriented along inter-rotorflux. The flux Ψ_2 induces a voltage E_2 in the short-circuited inter-rotor.

A. The inter-rotor in a field oriented reference frame

From (8), the torque can be written as

$$T_2 = \frac{3}{2} N_p \Psi_{2d} I_{2q} \tag{10}$$

The fluxes in (23) can be split up in their d-axis and the q-axis components. By combining (23) and (9), the following equation for the q-axis current in the inter-rotor is obtained:

$$I_{2q} = \frac{-1}{L_{22}} (L_{21} I_{1q} + L_{23} I_{3q}) \tag{11}$$

In order to control the torque, the flux thus has to be known. From the inter-rotor equation (2) and using definition (9):

$$p\Psi_{2d} = -R_2 I_{2d} \tag{12}$$

meaning that the resistive voltage drop equals the induced voltage in the inter-rotor. The torque T_2 is thus the multiplication of two orthogonal components Ψ_{2d} and I_{2q}. This is a result of the fact that the inter-rotor is short-circuited. Combining (12) with the definition of the inter-rotorflux (23) yields:

$$\Psi_{2d} = \frac{L_{21} I_{1d} + L_{23} I_{3d}}{1 + p\frac{L_{22}}{R_2}} \tag{13}$$

Note that in steady state, $I_{2d} = 0$. The denominator in (13) then becomes 1.

It is concluded that by considering the inter-rotor in this specific reference frame attached to the inter-rotor flux, the inter-rotor current from (11) and the inter-rotor flux from (13) can be written in terms of stator quantities, and so is the torque in (10).

B. The rotor in a field oriented reference frame

The torque on the rotor is given in (8) which is the cross product of Ψ_3 and I_3. The factor $L_{33} I_3$ in Ψ_3 does not contribute in this cross product (a winding cannot exert torque on itself) so:

$$T_3 = \frac{3}{2} N_p (I_{3q}(L_{31} I_{1d} + L_{32} I_{2d}) - I_{3d}(L_{31} I_{1q} + L_{32} I_{2q})) \tag{14}$$

C. Field oriented control

With the expressions above in a qd reference frame it's possible to derive a control scheme that controls the torque on both rotors. To this end the controller needs to select at every update instant a set of current vectors ($\underline{I}_1$,$\underline{I}_3$) satisfying the torque equations (10) and (14) respectively. Since there are only two torque equations to be fulfilled and four unknowns, two degrees of freedom remain. To this end also the inter-rotor flux Ψ_2 is controlled. There are several reasons to control the flux along with the torque:

- From (13) it can be seen that the flux cannot be changed instantaneously, which is a fundamental law of electromagnetism. In order to have a fast torque response without transient, the flux needs to be held at a certain value, as can be seen from (10) .
- The magnitude of the flux determines the degree of saturation. The inductances used in the equations are constant parameters determined in a certain operating point. In order for the torque control to be correct, the magnetization state of the machine cannot deviate too far from this point.
- Controlling the flux limits the current for a certain torque. More flux means that the torque-forming current component I_{2q} of the inter-rotor can be decreased, but that on the other hand the flux forming component I_{2d} of

the inter-rotor increases. The currents in the inter-rotor are directly related to the stator and rotor currents.
- The magnitude of the flux determines the back-emf of the machine. The voltage applied to the terminals of the machine is limited by the DC-bus voltage.

Summarized, the field oriented controller needs to select a set of current vectors ($\underline{I}_1$,$\underline{I}_3$) satisfying the following set of equations:

$$\begin{cases} \tau_2 = L_{21}I_{1q} + L_{23}I_{3q} \\ \Psi_{2d} = L_{21}I_{1d} + L_{23}I_{3d} \\ \tau_3 = L_{31}I_{1d}I_{3q} - I_{3d}(L_{31}I_{1q} + L_{32}I_{2q}) \end{cases} \tag{15}$$

with $\tau_2 = \frac{-2L_{22}}{3N_p\Psi_{2d}}T_2$, Ψ_{2d} and $\tau_3 = \frac{2}{3N_p}T_3$ known, and I_{2q} calculated in (11). Note that I_{2d} is zero and thus $p = 0$ in (13) because the flux is held at a constant value. Combining the equations leads to an equivalent set of equations:

$$\begin{cases} I_{3q} = \frac{\tau_2}{L_{23}} - \frac{L_{21}}{L_{23}}I_{1q} \\ I_{3d} = \frac{\Psi_{2d}}{L_{23}} - \frac{L_{21}}{L_{23}}I_{1d} \\ I_{1q} - a_2 I_{1d} = a_1 \end{cases} \tag{16}$$

with

$$\begin{cases} a_1 = -\frac{L_{23}\tau_3 + L_{32}\Psi_{2d}I_{2q}}{L_{31}\Psi_{2d}} \\ a_2 = \frac{L_{31}\tau_2 + L_{21}L_{32}I_{2q}}{L_{31}\Psi_{2d}} \end{cases} \tag{17}$$

Equation (16) shows that there is one degree of freedom left. This can be exploited to select the solution with the minimal joule losses. This leads to the following problem:

minimize

$$R_1 I_{1q}^2 + R_1 I_{1d}^2 + R_3(\frac{\tau_2}{L_{23}} - \frac{L_{21}}{L_{23}}I_{1q})^2 + R_3(\frac{\Psi_{2d}}{L_{23}} - \frac{L_{21}}{L_{23}}I_{1d})^2 \tag{18}$$

subjected to the constraint

$$I_{1q} - a_2 I_{1d} = a_1 \tag{19}$$

which can be solved using Lagrange multipliers. The solution is:

$$\begin{cases} I_{1q} = \frac{1}{h_1}(\lambda + h_2) \\ I_{1d} = \frac{1}{h_1}(-a_2\lambda + h_3) \\ I_{3q} = \frac{\tau_2}{L_{23}} - \frac{L_{21}}{L_{23}}I_{1q} \\ I_{3d} = \frac{\Psi_{2d}}{L_{23}} - \frac{L_{21}}{L_{23}}I_{1d} \end{cases} \tag{20}$$

with

$$\begin{cases} h_1 = 2R_1 + 2(\frac{L_{12}}{L_{23}})^2 R_3 \\ h_2 = 2\frac{L_{12}}{L_{23}^2}R_3\tau_2 \\ h_3 = 2\frac{\Psi_{2d}L_{12}}{L_{23}^2}R_3 \\ \lambda = \frac{a_1h_1 - h_2 + a_2h_3}{1+a_2^2} \end{cases} \tag{21}$$

In order to calculate the corresponding phase currents in the stator and rotor, the orientation of the qd-frame needs to be known. To this end an indirect field oriented control scheme can be used where the so-called slip equation is used to synchronize the currents with the field. Using (2) the pulsation of the field with respect to the inter-rotor (slippulsation) can be calculated:

$$s_2\omega = \frac{R_2 I_{2q}}{\Psi_{2d}} \tag{22}$$

with I_{2q} known from (11) and Ψ_{2d} from (13).

IV. Simulation

To support the theoretical derivations, simulations were performed in a Matlab-Simulink environment. A schematic overview of the simulated setup can be seen in Fig. 5. Starting from the setpoint values for flux and torque the setpoint currents are calculated in a qd-reference frame attached to the inter-rotor flux. Using indirect FOC the currents are translated to the corresponding phase currents. Using a predictive current controller the optimal gate signals (G) for the inverters are selected. The power electronic converters (PEC's) are ideal voltage source inverters, receiving their gate signals from a controller. The controller uses position feedback to locate the rotating magnetic field using indirect field oriented control. The position of the field is then used to transform the stator currents from the dq reference frame to the stationary stator frame, and the rotor currents to a reference frame rotating along with the rotor. Those currents are controlled using a predictive current controller. The motor parameters were identified using finite element calculations.

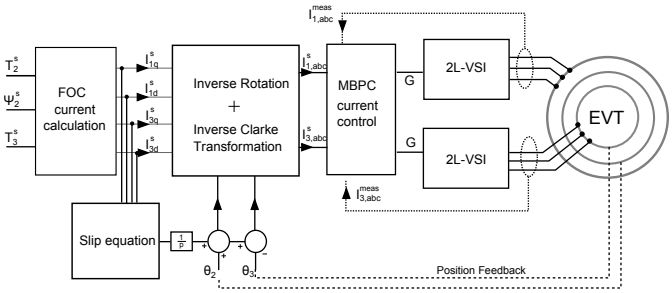

Fig. 5: Field Oriented Control Scheme for induction machine based EVT. The FOC current controller calculates the optimal set of currents needed to achieve the set point torque and flux values. Using the slip equation the calculated currents are transformed to the stator and rotor phase currents. Finally the phase currents are actually applied to the machine using a voltage source inverter and a dead beat current controller.

A. The Machine

The machine under consideration for simulations is based on the stator yoke of a 9kW induction machine. A geometrical optimization has been performed in order to select the width of the inter-rotor to achieve optimal efficiency. Finite element calculations have been performed to calculate the electromagnetic machine parameters. The machine parameters can be seen in table I. For the inter-rotor an equivalent wound rotor has been considered. Rated values are based on rated heat dissipation in a conventional induction machine of the same

power. The rated speed is based on the speed of the ICE and direct drive operation. The corresponding rated currents are given for the chosen number of windings depending on the inverter used.

TABLE I: rated machine parameters

	stator	inter-rotor	rotor
T_{rat} [Nm]	5	45	50
N_{rat} [rpm]	-	1500	1500
s_{rat} []	-	0.02	0.02
I_{rat} [A]	10	-	20
number of slots N_i	48	40	36
number of windings w_i	135	6.95	135
number of slots q_i per pole and per phase	4	$\frac{10}{3}$	3
number of pole pairs N_p	2	2	2
outer radius [mm]	120	74.3	64.3
inner radius [mm]	74.5	64.5	-
winding resistance [Ω]	0.51	0.000648	1.39

The inductance matrix from equation (23) is calculated as:

$$\begin{bmatrix} L_{11} & L_{12} & L_{13} \\ L_{12} & L_{22} & L_{23} \\ L_{13} & L_{23} & L_{33} \end{bmatrix} = \begin{bmatrix} 0.0858 & 0.00391 & 0.0815 \\ 0.00391 & 0.000185 & 0.00384 \\ 0.0815 & 0.00384 & 0.0891 \end{bmatrix} H \tag{23}$$

The machine can be characterized by a map of torque versus speed. This machine however has two rotors, so the torque - speed map is a four dimensional map. In order to have a two dimensional plot, the rotor speed is chosen to be 1500 rpm, which is a conventional ICE speed. The torque on the rotor (and the ICE) is chosen as such that the power to the wheels is entirely covered by the ICE power, so the battery is not used:

$$T_3\Omega_3 = T_2\Omega_2 + P_j(T_2, T_3) \tag{24}$$

This leaves only two variables: the torque T_2 and speed Ω_2 to the wheels. The resultant power and efficiency plot can be seen in Fig 6. For the efficiency calculations both joule and iron losses are taken into account. The flux is held at its maximum value corresponding to a flux density of 1.6T in the teeth. Only at high and low inter-rotor speed the flux has been weakened. The reason that the flux also needs to be weakened at low speeds is because the rotor voltage depends on the speed difference between inter-rotor and rotor as will be shown.

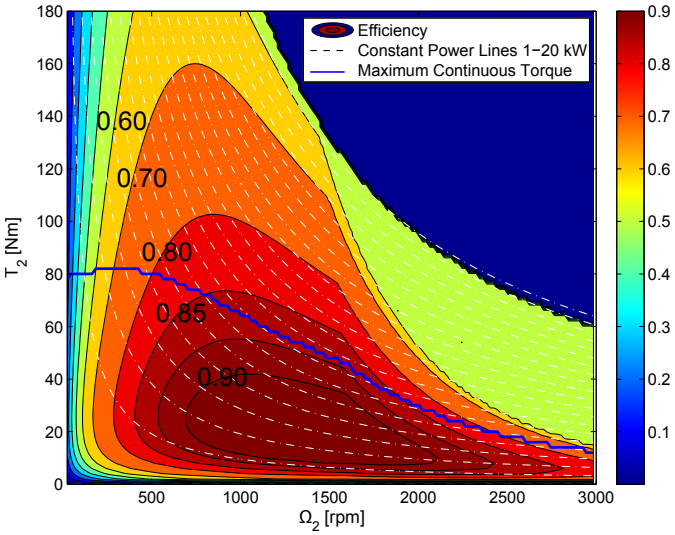

Fig. 6: Efficiency map. Ω_3 = 1500 rpm, $V_{dc} = 300V$.

The rated power of the machine is about 7kW, which is lower than the 9kW of an induction machine with the same stator. The reason for this is that the rotor diameter needs to be chosen lower because of the inter-rotor. This limits the maximum flux through the machine. The rotor slots can be chosen smaller but this increases the joule losses. This is an inherent disadvantage of this type of machine. Moreover heat removal will be harder because of the two rotors.

B. Choice of the inter-rotor flux

As mentioned in paragraph III-C the inter-rotor flux strongly influences the back-emf of the machine, the losses and the dynamical behaviour. The magnitude of the voltage induced in the stator and rotor windings can in sinusoidal steady-state be written as:

$$E_1 = \omega\Psi_1 = (s_2\omega + \omega_2)\Psi_1 \tag{25}$$

$$E_3 = s_3\omega\Psi_3 = (s_2\omega + \omega_2 - \omega_3)\Psi_3 \tag{26}$$

Every choice of inter-rotor flux Ψ_2 yields a set of current vectors ($\underline{I}_1$,$\underline{I}_3$), the solution of (20). Every solution gives rise to a unique slip pulsation and set of fluxes and thus determines the induced voltages. Further E_1 depends linearly on the speed of the inter-rotor, while E_3 depends linearly on the difference in speed of inter-rotor and rotor as can be seen in (25) and (26) respectively. At the terminals of the machine the resistive voltage drop over the windings is added to the induced voltage as can be seen in equations (1) and (3). This resistive part is mainly of interest when the torque is high or the flux level of the machine is low since then high currents are demanded. However, in most operating points the influence is negligible. Then the relation between voltage V_1 and speed ω_2 or between V_3 and speed difference $\omega_3 - \omega_2$ is linear and is characterized by the voltage at zero speed and its slope. The voltage at zero speed is determined by the slip pulsation $s_2\omega$ which is a function of the inter-rotor torque using equations (10) and (22):

$$s_2\omega = \frac{2R_2}{3N_p}\frac{T_2}{\Psi_{2d}^2} \tag{27}$$

The reason for this is that a current needs to be induced in the inter-rotor in order to have an electromagnetic torque. To this end an alternating magnetic field is required, thus a slip pulsation. The lower the inter-rotor flux is chosen, the more current needs to be induced in the inter-rotor bars in order to have the same torque. Thus the lower the inter-rotor flux, the higher the slip pulsation, and thus the voltage at zero speed. With increasing speed or speed difference, the voltages increase almost linearly with slope Ψ_1 and Ψ_3 respectively as can be seen in equations (25) and (26) . If the stator voltage is the limiting factor, equation (25) combined with equation (27) gives the maximum inter-rotor speed.

$$\omega_{2,max} = \frac{V_{max}}{\Psi_1} - \frac{2R_2T_2}{3N_p}\frac{1}{\Psi_2^2} \tag{28}$$

The same can be done if the rotor voltage is the limiting factor by using equation (26):

$$\omega_{2,max} = \frac{V_{max}}{\Psi_3} - \frac{2R_2T_2}{3N_p}\frac{1}{\Psi_2^2} + \omega_3 \tag{29}$$

with V_{max} the maximum achievable voltage, which is equal to $\frac{V_{dc}}{\sqrt{3}}$ since space vector modulation is used to synthesize the voltage vectors. Fig. 7a shows the relation between maximum speed and inter-rotor flux for a specific operating point for both the stator and rotor voltage as limiting factor. Starting form maximum flux level and weakening the flux, the maximum achievable speed or speed difference increases as can be expected. However at a specific flux level a maximum is reached and the achievable speed drops. This has two main reasons. First the influence of leakage fields on the stator and rotor play an important role at low inter-rotor flux level. The third curve in the plot represents the speed relation for stator and rotor if no leakage were present, so that $\Psi_1 = \Psi_2 = \Psi_3$ in equations (28) and (29). The leakage fields thus strongly decrease the maximum speed. The other important factor is that the influence of the slip pulsation becomes dominant at low inter-rotor flux as explained before. If the ICE speed Ω_3 is assumed to be held constant at 1500 rpm, and by taking the most strict limitation of stator and rotor voltage, the speed-flux range of Fig. 7b results.

Also the joule losses are given which decrease towards higher flux for this operating point. For part load the minimum joule losses are possibly situated at flux levels lower that $\Psi_{2,max}$. This is however dynamically not always achievable since flux cannot be changed instantaneously. The flux range lower than $\Psi_{2,min}$ as given in Fig. 7b is not of interest for this operating point since the same speed can be achieved at higher flux and thus lower losses. It is concluded that the flux reference for the inter-rotor is chosen to be as high as possible, except when the speed is too high or low.

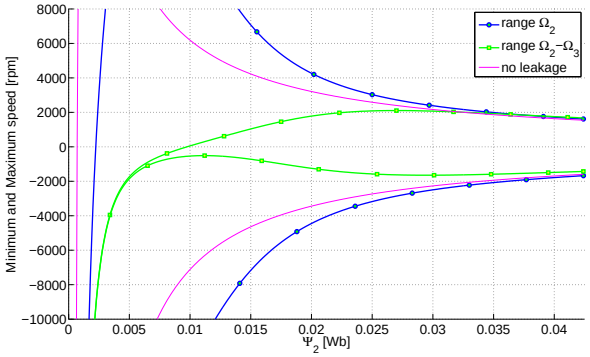

(a) Speedrange of inter-rotor Ω_2 if the stator voltage is the limiting factor, and speed range of inter-rotor with respect to rotor $\Omega_2 - \Omega_3$ if the rotor voltage is limiting factor.

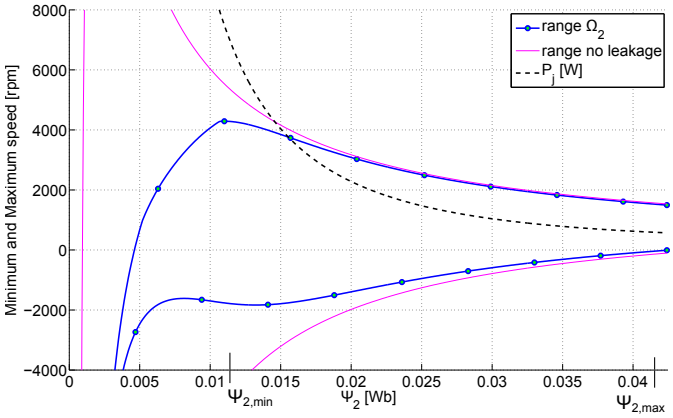

(b) Speed range of inter-rotor if ICE speed $\Omega_3 = 1500$rpm. Also joule losses P_j are given.

Fig. 7: Choice of the inter-rotor flux, simulation result. T_2 = 45Nm, T_3 = -50Nm, V_{dc} = 500V.

C. Current control

The control scheme derived above gives the reference values for the stator and rotor currents. Those currents however cannot directly be applied to the terminals of the machine since only the voltages can be steered. To this end a current controller is needed in order to select at every instant the optimal voltage vector that needs to be applied to the machine in order to track the current reference as accurately as possible. Since an EVT forms a MIMO system to be controlled, a predictive current controller is particularly attractive. Deadbeat Current Control is a specific type of model based predictive control (MBPC) that can be used to control several outputs. Suppose the present time t is equal to $kT_u, k \in \mathbb{Z}$ with T_u the controller update period. At this moment an optimal switching sequence S^k is applied to the inverters. This switching sequence was calculated in the previous time interval. The goal is now to calculate the next switching sequence to be applied at $t = (k+1)T_u$ till $t = (k+2)T_u$. The calculation of this switching state happens in the interval from $t = kT_u$ to $t = (k+1)T_u$. The algorithm

can be divided into three main steps:

1) Estimation: The state of the currents at $t = (k+1)T_u$ is fixed because of the switching sequence $S(k)$, but is not know at the current moment kT_u. To this end the currents at $t = (k+1)T_u$ are estimated using the model of the EVT. For the calculations to be carried out in a controller, the model is discretized and a first order Euler approximation is used. The time derivatives of the currents at kT_u are calculated using as initial conditions the measurements of the currents at $t = kT_u$. Also the flux is needed to specify the state of the machine at this moment. This is done by estimating the flux using equations (1) and (3). The voltage is known since the switching state is known.
2) Prediction: Using the inverse discretized model, the voltages needed to force the currents on their reference current at $t = (k+2)T_u$ are calculated. To this end the estimated currents and fluxes at $t = (k+1)T_u$ are used.
3) Modulation: since the voltage source inverters are used, only a set of discrete voltage vectors can be applied to the machine. In order to synthesize the desired voltage vectors from the prediction step, a space vector modulation is used. Using this modulation principle the voltage vectors applied to the machine terminals are on average equal to the desired voltage vectors over the controller time interval.

D. Simulation

The simulation results aim to show how FOC can accurately control the inter-rotor flux and the torque on both rotors in different working conditions. The simulation consists of five parts as can be seen in Fig. 9a. First both rotors are in no-load condition. The inter-rotor speed Ω_3 is equal to the ICE speed and is assumed to be held constant at 1500rpm. The energy withdrawn from the battery plotted in Fig. 8 is used to keep the machine magnetized at the predefined inter-rotor flux level, which is shown in Fig. 11a. To this end a dc current is sent through the stator in Fig. 10a and an alternating current through the rotating rotor in Fig. 10b. The frequency of the current is equal to the rotational speed of the rotor in order to maintain a stationary magnetic field. Consequently no currents are induced in the inter-rotor as can be seen in Fig. 11b and the torque on the inter-rotor is zero. From $t = 50$ms a torque reference is imposed on the inter-rotor, while the torque on the rotor remains zero. This corresponds to EV-mode of a hybrid vehicle, with the power entirely delivered by the battery. A q-axis current is induced in the inter-rotor since the magnetic field is forced to have a certain slip with respect to the inter-rotor bars. The torque tracks the reference very accurately, and steps are tracked without overshoot with this predictive current controller. The torque ripple is about 1% of the reference torque as can be seen in the figure and is due to the current regulation. In the simulation the controller has perfect knowledge of the machine parameters. In the third simulation stage from $t = 100$ms the ICE is loaded with a negative torque in order to transmit the ICE power and charge the battery. From $t = 150$ms the torque to the wheels is tripled so that the battery needs to assist the ICE. Finally from $t = 200$ms a negative torque is imposed on the inter-rotor and regenerative braking is used to charge the battery and slow the inter-rotor down. As such the different operation modes of the EVT are illustrated.

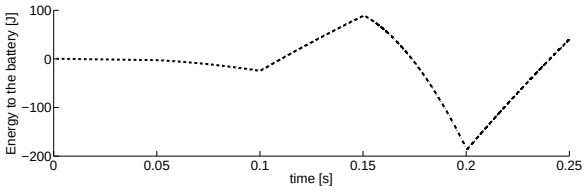

Fig. 8: Energy fed to the battery, corresponding to the battery state of charge.

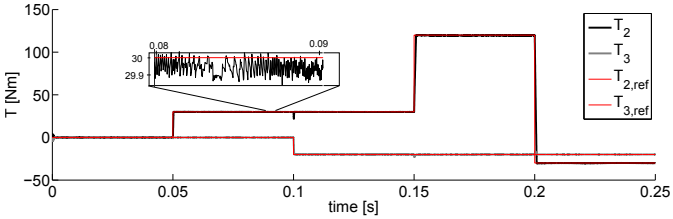

(a) Torque on the inter-rotor and rotor of an induction machine based EVT.

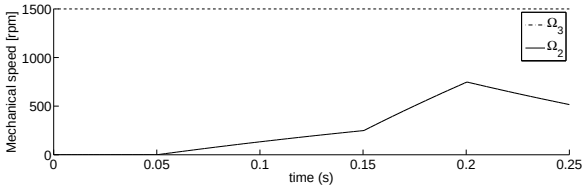

(b) Mechanical speed of inter-rotor and rotor.

Fig. 9: Field Oriented Control, simulation result.

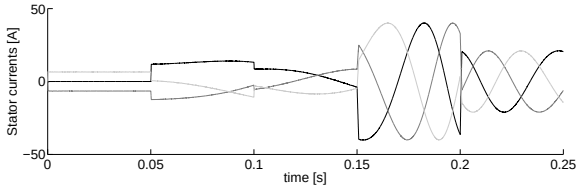

(a) Stator currents applied via PEC1.

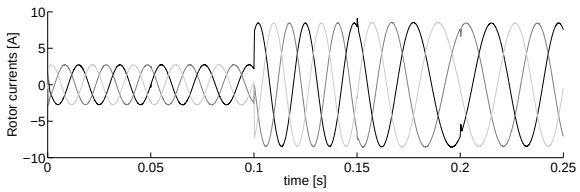

(b) Currents through the rotor, applied via the slip rings and PEC3.

Fig. 10: Currents controlled by the current controller.

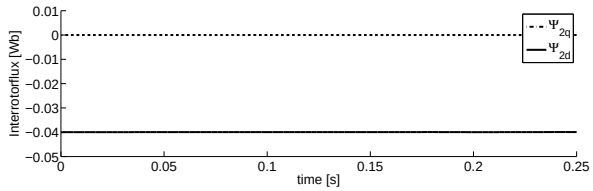

(a) inter-rotor flux

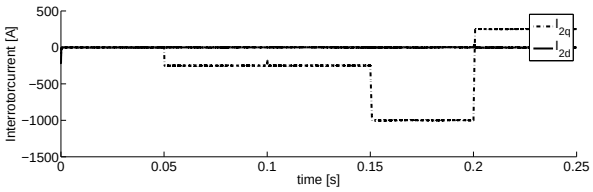

(b) Induced inter-rotor currents.

Fig. 11: inter-rotor quantities in a synchronous qd-reference frame.

V. Validation using Transient Finite Element Calculations

A. Finite Element Analysis

In order to validate the torque control technique, finite element calculations were performed. The analysis is performed in 2D and consists of a mesh with 492589 nodes, of with the density is highest in the two air gaps. The simulations is time-transient with 0.4ms time steps. The material is considered linear, but the flux is chosen as such that the flux density in the teeth never exceeds 1.6T. The first two torque steps of Fig. 9a where applied as setpoint. A field oriented torque controller calculates the desired phase currents, which are then directly applied to the windings of the machine (ideal current regulation). The speed of both rotor and inter-rotor are assumed to be held constant over the calculated time interval at 1500rpm and 1000rpm respectively. The torque is calculated using the Maxwell stress harmonic filter method from [29]. According to Maxwell's stress tensor the electromagnetic torque on a rotor can be written as

$$T = \frac{1}{\mu_0} \int_0^{2\pi} r^2 B_r B_\theta d\theta \tag{30}$$

where B_r and B_θ are calculated from the derivatives of the magnetic vector potential A_z to θ and r respectively. Consequently the induction waveforms are an order less accurate than the vector potential that evolves linearly in the triangular mesh elements. To cope for this issue the vector potential is written in terms of a Fourier series and is then analytically derivated. This way an analytical solution for (30) can be found as function of the Fourier coefficients of the vector potential along two circles in the air gap.

B. Finite Element Results

The simulation is, depending on the torque setpoint, divided into three parts. The first 40ms both torque setpoints are zero and the controller maintains the flux in the machine. The magnetic field rotates along with the inter-rotor since the slip pulsation is zero. In the stator a rotating current layer is applied rotating at the speed of the inter-rotor, so with frequency of 33.3Hz. Since the rotor rotates at 500 rpm with respect to the inter-rotor, currents are applied with a frequency of 16.6Hz and with reversed phase order. The applied currents can be seen in Fig. 12a and Fig. 12b where the current density is plotted. Also the corresponding current and flux waveforms in space are given. The inter-rotor current is converted to the number of windings of the stator. Every circular marker on the figure represents one inter-rotor bar. The stator and rotor currents are at every moment in phase with the inter-rotorflux. The fundamental harmonic of the induced inter-rotor current is zero so no net torque is imposed on the inter-rotor as can also be seen in Fig. 13. Higher space harmonic current components of order 3, 5, 7 and 9 are present, which are due to the stator and rotor mmf waveform. At $t = 40$ms a torque step of 30Nm is given to the inter-rotor. The applied currents to stator and rotor induce a fundamental q-axis current in the inter-rotor. This can be seen in Fig. 12c where the induced inter-rotor current is 90° shifted with respect to the field. Finally at $t = 60$ms a torque on the rotor is imposed by shifting the rotor currents with respect to the induced magnetic field as can be seen in Fig. 12d. Fig. 14 shows the induced inter-rotor currents in a qd-reference frame. The ripple is due to the effect of slotting on the airgap field. Harmonics due to the stator and rotor slots can be observed in the currents induced in the inter-rotor bars.

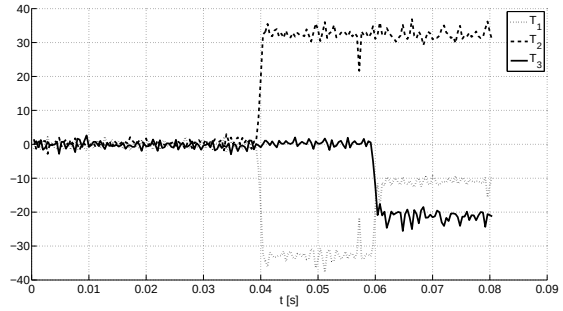

Fig. 13: Electromagnetic Torque, Transient Finite Element Calculations

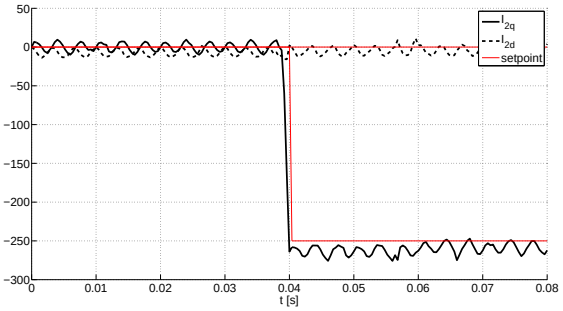

Fig. 14: Induced inter-rotor current, Transient Finite Element Calculations

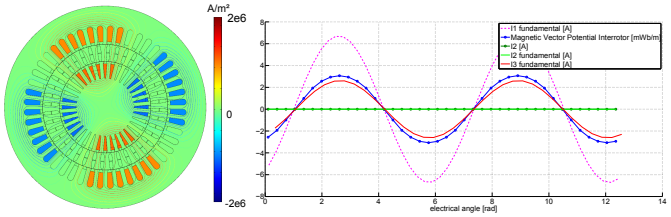

(a) t = 0ms

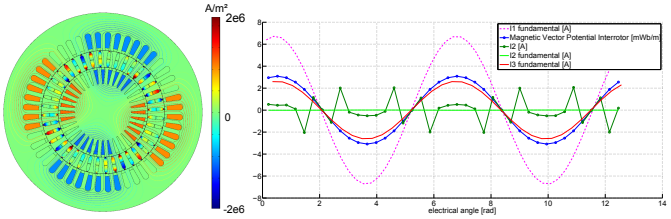

(b) t = 20ms

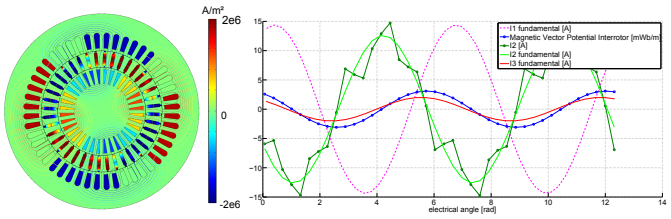

(c) t = 45ms

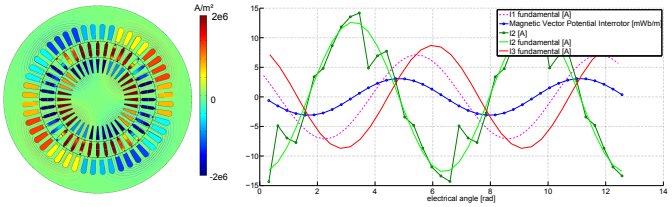

(d) t = 70ms

Fig. 12: Transient 2D finite element calculation results showing the applied and induced current densities (left) and the corresponding spacial current and flux wave forms (right).

VI. Conclusion

In this paper an induction machine based EVT has been considered. This type of machine has the advantage that no expensive magnets are needed. Also the irreversible demagnetization risk of magnets is avoided and the magnetic field can easily be weakened at high speeds. The proposed field oriented controller calculates at every update instant a set of stator and rotor currents in order to control the torque on both rotors along with the inter-rotor flux. The additional degree of freedom in the set of torque and flux equations is used to minimize the joule losses. Also the inter-rotor flux is chosen so that the limited battery voltage is taken into account along with the joule losses. Finally, computer simulations and finite element calculations are performed for an EVT based on a 9kW induction machine. It shows that a field oriented controller in combination with a deadbeat current controller can accurately control the torque and flux of an EVT in different operating points. It is also illustrated that this kind of machine can be used to transmit power, to generate electrical energy and to work in full electric mode with the proposed controller.

References

[1] E. Hesla, "Electric propulsion [history]," *Industry Applications Magazine, IEEE*, vol. 15, no. 4, pp. 10–13, July 2009.

[2] F. Ju, J. Wang, J. Li, G. Xiao, and S. Biller, "Virtual battery: A battery simulation framework for electric vehicles," *Automation Science and Engineering, IEEE Transactions on*, vol. 10, no. 1, pp. 5–15, Jan 2013.

[3] Y. Cheng, R. Trigui, C. Espanet, A. Bouscayrol, and S. Cui, "Specifications and design of a pm electric variable transmission for toyota prius ii," *Vehicular Technology, IEEE Transactions on*, vol. 60, no. 9, pp. 4106–4114, Nov 2011.

[4] E. Vinot, R. Trigui, Y. Cheng, C. Espanet, A. Bouscayrol, and V. Reinbold, "Improvement of an evt-based hev using dynamic programming," *Vehicular Technology, IEEE Transactions on*, vol. 63, no. 1, pp. 40–50, Jan 2014.

[5] K. van Berkel, T. Hofman, B. Vroemen, and M. Steinbuch, "Optimal control of a mechanical hybrid powertrain," *Vehicular Technology, IEEE Transactions on*, vol. 61, no. 2, pp. 485–497, Feb 2012.

[6] L. Chen, F. Zhu, M. Zhang, Y. Huo, C. Yin, and H. Peng, "Design and analysis of an electrical variable transmission for a series parallel hybrid electric vehicle," *Vehicular Technology, IEEE Transactions on*, vol. 60, no. 5, pp. 2354–2363, Jun 2011.

[7] T. Hofman, S. Ebbesen, and L. Guzzella, "Topology optimization for hybrid electric vehicles with automated transmissions," *Vehicular Technology, IEEE Transactions on*, vol. 61, no. 6, pp. 2442–2451, July 2012.

[8] M. Hoeijmakers and M. Rondel, "The electrical variable transmission in a city bus," in *Power Electronics Specialists Conference, 2004. PESC 04. 2004 IEEE 35th Annual*, vol. 4, 2004, pp. 2773–2778 Vol.4.

[9] K. Atallah, J. Wang, S. Calverley, and S. Duggan, "Design and operation of a magnetic continuously variable transmission," *Industry Applications, IEEE Transactions on*, vol. 48, no. 4, pp. 1288–1295, July 2012.

[10] L. Jian and K. Chau, "Design and analysis of a magnetic-geared electronic-continuously variable transmission system using finite element method," *Progress in electromagnetic research*, vol. 107, pp. 47–61, 2010.

[11] Y. Zhu, M. Cheng, W. Hua, and B. Zhang, "Sensorless control strategy of electrical variable transmission machines for wind energy conversion systems," *Magnetics, IEEE Transactions on*, vol. 49, no. 7, pp. 3383–3386, July 2013.

[12] P. Pisek, B. Stumberger, T. Marcic, and P. Virtic, "Design analysis and experimental validation of a double rotor synchronous pm machine used for hev," *Magnetics, IEEE Transactions on*, vol. 49, no. 1, pp. 152–155, Jan 2013.

[13] K. Atallah and D. Howe, "A novel high-performance magnetic gear," *Magnetics, IEEE Transactions on*, vol. 37, no. 4, pp. 2844–2846, Jul 2001.

[14] E. Gouda, S. Mezani, L. Baghli, and A. Rezzoug, "Comparative study between mechanical and magnetic planetary gears," *Magnetics, IEEE Transactions on*, vol. 47, no. 2, pp. 439–450, Feb 2011.

[15] R. Montague, C. Bingham, and K. Atallah, "Servo control of magnetic gears," *Mechatronics, IEEE/ASME Transactions on*, vol. 17, no. 2, pp. 269–278, April 2012.

[16] P. Rasmussen, T. Frandsen, K. Jensen, and K. Jessen, "Experimental evaluation of a motor-integrated permanent-magnet gear," *Industry Applications, IEEE Transactions on*, vol. 49, no. 2, pp. 850–859, March 2013.

[17] X. Sun, M. Cheng, W. Hua, and L. Xu, "Optimal design of double-layer permanent magnet dual mechanical port machine for wind power application," *Magnetics, IEEE Transactions on*, vol. 45, no. 10, pp. 4613–4616, Oct 2009.

[18] L. Xu, Y. Zhang, and X. Wen, "Multioperational modes and control strategies of dual-mechanical-port machine for hybrid electrical vehicles," *Industry Applications, IEEE Transactions on*, vol. 45, no. 2, pp. 747–755, March 2009.

[19] M. Hoeijmakers and J. Ferreira, "The electric variable transmission," *Industry Applications, IEEE Transactions on*, vol. 42, no. 4, pp. 1092–1100, July 2006.
[20] M. Hoeijmakers, "Electromechanical converter," Jan. 16 2007, uS Patent 7,164,219. [Online]. Available: http://www.google.co.in/patents/US7164219
[21] C. Shumei, H. Wenxiang, C. Yuan, N. Kewang, and C. Chan, "Design and experimental research on induction machine based electrical variable transmission," in *Vehicle Power and Propulsion Conference, 2007. VPPC 2007. IEEE*, Sept 2007, pp. 231–235.
[22] X. Sun and M. Cheng, "Thermal analysis and cooling system design of dual mechanical port machine for wind power application," *Industrial Electronics, IEEE Transactions on*, vol. 60, no. 5, pp. 1724–1733, May 2013.
[23] J. Druant, P. Sergeant, F. De Belie, and J. Melkebeek, "Modeling and control of an induction machine based electrical variable transmission," in *IEEE International Conference on Electrical Machines*, Sept 2014, pp. 1–6.
[24] J. Kim, T. Kim, B. Min, S. Hwang, and H. Kim, "Mode control strategy for a two-mode hybrid electric vehicle using electrically variable transmission (evt) and fixed-gear mode," *Vehicular Technology, IEEE Transactions on*, vol. 60, no. 3, pp. 793–803, March 2011.
[25] Y. Murphey, J. Park, L. Kiliaris, M. Kuang, M. Masrur, A. Phillips, and Q. Wang, "Intelligent hybrid vehicle power control;part ii: Online intelligent energy management," *Vehicular Technology, IEEE Transactions on*, vol. 62, no. 1, pp. 69–79, Jan 2013.
[26] M. Choi, J. Lee, and S. Seo, "Real-time optimization for power management systems of a battery/supercapacitor hybrid energy storage system in electric vehicles," *Vehicular Technology, IEEE Transactions on*, vol. 63, no. 8, pp. 3600–3611, Oct 2014.
[27] Z. Chen, C. Mi, J. Xu, X. Gong, and C. You, "Energy management for a power-split plug-in hybrid electric vehicle based on dynamic programming and neural networks," *Vehicular Technology, IEEE Transactions on*, vol. 63, no. 4, pp. 1567–1580, May 2014.
[28] V. P., in *Electrical Machines and Drives: A Space-Vector Theory Approach*. Osford University Press, 1992.
[29] M. Popescu, "Prediction of the electromagnetic torque in synchronous machines through maxwell stress harmonic filter (hft) method," *Electrical Engineering*, vol. 89, no. 2, pp. 117–125, 2006. [Online]. Available: http://dx.doi.org/10.1007/s00202-005-0323-1

Joachim Druant was born in Ieper, Belgium on February 19, 1990. He received the M.Sc. degree in electromechanical engineering in 2013 from Ghent University, Ghent, Belgium. Since then, he has been with the Electrical Energy Laboratory (EELAB), Department of Electrical Energy, Systems and Automation (EESA) of Ghent University and is currently working towards a Ph.D. degree. In 2014, he was awarded a Ph.D. Fellowship from the Research Foundation-Flanders (FWO). His present research interests include digital control of converter-fed electrical machines, fault tolerant control, and modeling and control on electrical variable transmissions.

Frederik De Belie was born in Belgium in 1979. He received the Master degree in electromechanical engineering from Ghent University, Ghent, Belgium, in 2002, and the Ph.D. degree in March 2010. He's currently a post-doctoral assistant in the Electrical Energy, Systems and Automation Department of the Ghent University. His present research interests include modelling theory and control-system theory applied to electrical drives and, in particular, self-sensing control of synchronous machines.

Peter Sergeant received the M.Sc. degree in electromechanical engineering in 2001, and the Ph.D. degree in engineering sciences in 2006, both from Ghent University, Ghent, Belgium. In 2001, he became a researcher at the Electrical Energy Laboratory of Ghent University. He became a postdoctoral researcher at Ghent University in 2006 (postdoctoral fellow of the Research Foundation - Flanders) and at Ghent University College in 2008. Since 2012, he is associate professor at Ghent University. His current research interests include numerical methods in combination with optimization techniques to design nonlinear electromagnetic systems, in particular, electrical machines for sustainable energy applications.

Jan Melkebeek was born in Gent, Belgium on February 20, 1952. He received the 'Ingenieur' degree in electrical and mechanical engineering from the University of Gent, Belgium in 1975, and the degree of Doctor in Applied Sciences from the same university in 1980. In 1986 he obtained the degree of 'Doctor Habilitus' in Electrical and Electronical Power Technology. Since 1987 he is Professor in Electrical Engineering at the Engineering Faculty of the University of Gent. He is the head of the Department of Electrical Power Engineering, Systems and Automation and the director of the Electrical Energy Laboratory (EELAB). Prof. Melkebeek is a fellow of the IEE and a senior member of the IEEE. He served as the president of the IEEE Benelux IAS-PELS joint chapter from 2002 to 2003 and is a long-time member of the IEEE-IAS Electric Machines Committee, the IEEE-IAS Electric Drives Committee and of the IEEE-PES Machine Theory Subcommittee.